The Electrochemical Society
Advancing solid state & electrochemical science & technology

Glyme-Lithium Bis(trifluoromethylsulfonyl)amide Super-concentrated Electrolytes: Salt Addition to Solvate Ionic Liquids Lowers Ionicity but Liberates Lithium Ions

View the article online for updates and enhancements.

Glyme-Lithium Bis(trifluoromethylsulfonyl)amide Super-concentrated Electrolytes: Salt Addition to Solvate Ionic Liquids Lowers Ionicity but Liberates Lithium Ions

Atsushi Kitada,[1,z] Yoshiki Koujin,[1] Masahiro Shimizu,[2,*] Kio Kawata,[1] Chiaki Yoshinaka,[1] Masayuki Saimura,[3] Takashi Nagata,[3] Masato Katahira,[3] Kazuhiro Fukami,[1,*] and Kuniaki Murase[1,*]

[1]Department of Materials Science and Engineering, Kyoto University, 36-1 Yoshida-hommachi, Sakyo-ku, Kyoto 606-8501, Japan
[2]Department of Materials Chemistry, Faculty of Engineering, Shinshu University, 4-17-1 Wakasato, Nagano 380-8553, Japan
[3]Institute of Advanced Energy, Kyoto University, Gokasho, Uji, Kyoto 611-0011, Japan

Solvate ionic liquids (ILs) such as binary equimolar mixtures of glymes (ethyleneglycol-dimethylether or $CH_3(OCH_2CH_2)_nOCH_3$) and lithium bis(trifluoromethylsulfonyl)amide ($LiTf_2N$; $Tf = SO_2CF_3$) are known to show identical self-diffusion coefficients for glymes and Li^+ ions. Here, we report that the addition of $LiTf_2N$ to the solvate ILs drastically changes their electrolyte properties. When the lithium salts are added to give the super-concentrated electrolytes with $[O]/[Li^+] = 3$ (molar ratio of ether oxygen to Li^+), ligand exchange or hopping conduction of Li^+ takes place for triglyme (G3; $n = 3$) and tetraglyme (G4; $n = 4$). In addition, the Li^+ transference number $t_{Li+(EC)}$, electrochemically measured under anion blocking conditions, increases about 3–6 times compared with the solvate ILs. Consequently, segmental motion of glymes apparently affects the transport properties even for the shorter G3 in the super-concentrated region. The relationship between the coordination structure and the transport properties are also discussed as a function of ionicity, the extent of the contribution of self-diffusion to the actual ion conduction. Plots vs ionicity demonstrate that a clear line can be drawn between the solvate ILs and the super-concentrated electrolytes.
© 2021 The Author(s). Published on behalf of The Electrochemical Society by IOP Publishing Limited. This is an open access article distributed under the terms of the Creative Commons Attribution 4.0 License (CC BY, http://creativecommons.org/licenses/by/4.0/), which permits unrestricted reuse of the work in any medium, provided the original work is properly cited. [DOI: 10.1149/1945-7111/ac239c]

Highly concentrated electrolytes have been studied for various kinds of electrochemical applications such as next-generation batteries,[1–12] fuel cells,[13–18] and surface finishing.[19–22] Compared to conventional electrolytes with normal salt concentrations, a practical merit is safety, especially in the cases of non-aqueous media, because vapor pressure of solvent is lowered and electrochemical stability is extended. The wider electrochemical windows also improve cycling performance of energy devices and electrochemical deposition/dissolution behaviors of metals. Besides, the non-conventional transport properties of highly concentrated electrolytes attract fundamental interest. For instance, ligand exchange or hopping conduction of ions, which means that ions move faster than solvents or ligands, is striking.[7–16]

Glymes are oligoethers denoted as $CH_3(OCH_2CH_2)_nOCH_3$ ($n = 1, 2, 3, 4, 5,…$), which have $n + 1$ ether oxygens per molecule. Some equimolar mixtures of glyme-lithium salt with weakly Lewis basic anions (e.g., bis(perfluorosulfonyl)amide anions) do not possess free glymes. Such equimolar mixtures are classified as solvate ionic liquids (ILs), which have been expected as promising battery electrolytes.[2–5] In $[Glyme]/[LiTf_2N] = 1/1$, where $LiTf_2N$ ($Tf = SO_2CF_3$) denotes lithium bis(trifluoromethylsulfonyl)amide, each Li^+ ion is solvated to each glyme ligands, giving the same self-diffusion coefficients ($D_{Li+}/D_{glyme} = 1$; strictly 0.9–1.1): this means the hopping conduction is absent in the bulk electrolyte;[6,23,24] notably, at the electrode/electrolyte interface a specific ligand-exchange Li^+ conduction mechanism was proposed.[3,23]

Very recently, however, the first example of a glyme system which shows Li^+ hopping conduction in the bulk electrolyte was reported.[12] The system was room temperature liquid $[G5]/[LiTf_2N] = 1/2$ with $[O]/[Li^+] = 3$ (molar ratio of ether oxygen to Li^+). Since the average coordination number of Li^+ is 4 or 5,[23] the number of solvent molecules is not enough to solvate all of the metal ions at $[O]/[Li^+] = 3$. Thus, Tf_2N^- anions participate in the coordination of Li^+ cations as well as G5 solvents. Also, it has been considered that bridging of the cations by the anions and the ligands plays a key role for the hopping conduction in the highly concentrated solutions.[7–11] On the other hand, a shorter glyme system of $[O]/[Li^+] = 3$ with the identical ratio, i.e. $[G2]/[LiTf_2N] = 1/1$, do *not* show hopping conduction.[12] The comparison of G5 and G2 systems clarifies that glyme chain length or number of ether oxygens per glyme is important for the conduction mechanism.

Herein, we focus on glyme length, $[O]/[Li^+]$ ratio, and $[Gn]/[LiTf_2N]$ ratio, in order to systematically understand the ion conduction of the glyme-$LiTf_2N$ systems. Glyme-$LiTf_2N$ with the ratio $[O]/[Li^+] = 3$, i.e. $[G3]/[LiTf_2N] = 3/4$ and $[G4]/[LiTf_2N] = 3/5$ are studied and compared with the previous studies on the G5 analogue and solvate ILs.[6,12,23,24] In this article, the series of $[O]/[Li^+] = 3$ are called super-concentrated electrolytes. It is revealed that among the super-concenrated electrolytes hopping conduction takes place except the G2 compound. Their static (structure) and dynamic (transport) properties are compared to show that the magnitude of D_{Li+}/D_{glyme} is in the order G5 > G3 > G4, which can be explained by the strengths of Li^+-solvent and Li^+-Tf_2N^- interactions as revealed by the Raman and 1D NMR spectra. Also, ionicity, the extent of contribution of self-diffusion to the actual ion conduction, is utilized to classify the glyme-$LiTf_2N$ systems. The super-concentrated electrolytes show high transference numbers and low ionicity, whereas the solvate ILs show low transference numbers and high ionicity.

Experimental

Lithium bis(trifluoromethylsulfonyl)amide ($LiTf_2N$; Kishida chemical, 99.9% purity) and glymes (diglyme (G2), triglyme (G3), tetraglyme (G4), pentaglyme (G5); Nippon Nyukazai Co., >99% purity) were used as reagents. Before preparing electrolyte solutions, $LiTf_2N$ was dried by heating at 100 °C for 24 h under Ar atmosphere, and glymes were dried using molecular sieves (3 A).

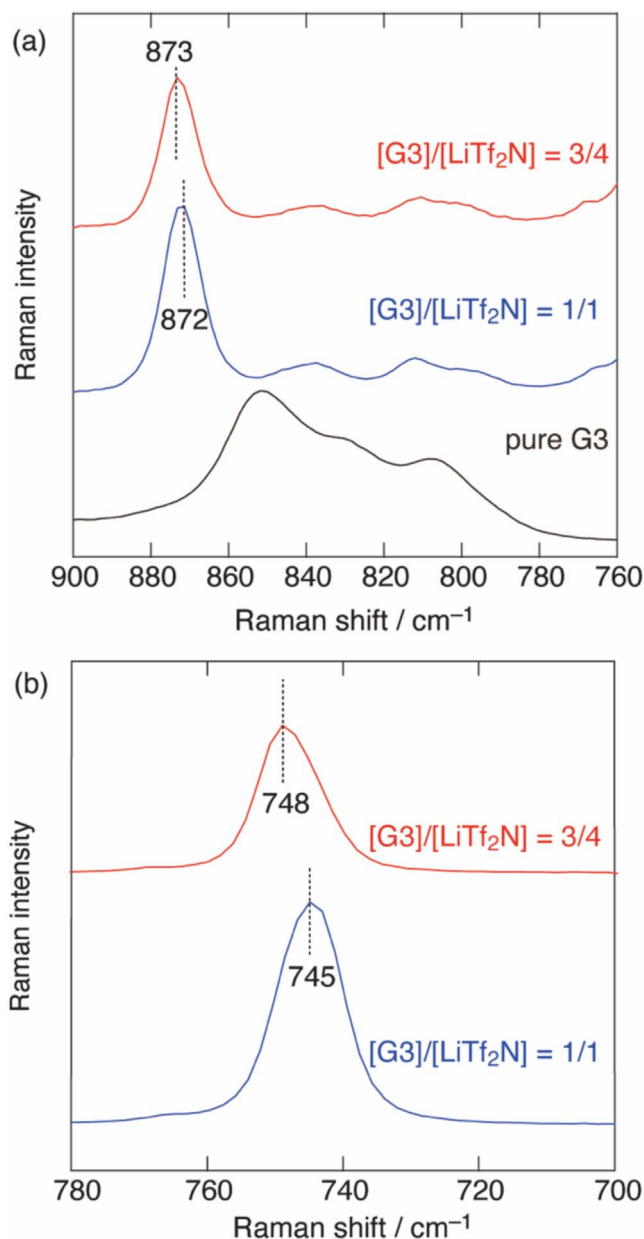*Electrochemical Society Member
zE-mail: kitada.atsushi.3r@kyoto-u.ac.jp

Figure 1. Raman spectra for pure G3 and the molten states of [G3]/[LiTf$_2$N] = 1/1 and 3/4: wavenumber regions characteristic for (a) glymes and (b) Tf$_2$N$^-$ anions. Dashed lines are guide to the eye.

After adding stoichiometric amount of LiTf$_2$N to glymes, [G3]/[LiTf$_2$N] = 3/4 and [G4]/[LiTf$_2$N] = 3/5 were stirred at 600 rpm at 80 °C for 6 h for complete dissolution. To compare Raman and NMR spectra, other samples with different mixing ratio, i.e., [G3]/[LiTf$_2$N] = 1/1 and [G4]/[LiTf$_2$N] = 1/1 were prepared through agitation at 500 rpm at 65 °C for 6 h. In addition, [G2]/[LiTf$_2$N] = 1/1 and [G5]/[LiTf$_2$N] = 1/1 were prepared to obtain their transference numbers and/or conductivities; the conductivity of [G5]/[LiTf$_2$N] = 1/1, 7.75 mS cm^{-1} at 90 °C, was used to calculate its ionicity (see Results and Discussions) using the literature values of the self-diffusion coefficients.[12] [G2]/[LiTf$_2$N] = 1/1 was stirred at 500 rpm at 65 °C for 6 h, and [G5]/[LiTf$_2$N] = 1/1 at 750 rpm at 100 °C for 4 h.

Thermogravimetry (TG) was conducted using a differential scanning calorimeter (Rigaku, TG-DTA8122) with the scan rate of 5 °C min^{-1}. 10 mg sample was packed in Al pan. Al$_2$O$_3$ was used as a standard. Also, the glass transition temperature of [G3]/[LiTf$_2$N] = 3/4

and [G4]/[LiTf$_2$N] = 3/5 were determined using a differential scanning calorimeter (DSC; Rigaku, DSC8231) with the scan rate of 5 °C min^{-1} using Al pans and 10.0 mg Al$_2$O$_3$ standard samples.

Raman spectroscopy was performed at molten states for [G3]/[LiTf$_2$N] = 3/4 (at 70 °C) and [G4]/[LiTf$_2$N] = 3/5 (at 80 °C). For these measurements, an integrated Raman system (B&W Tek, InnoRam 785) was used, which consist of a semiconductor laser light source (785 nm), an axial transmissive spectrograph, a holographic probe head, and a CCD detector.

One-dimensional NMR (^{1}H and ^{7}Li) and PFSE-NMR (^{1}H, ^{7}Li, and ^{19}F) measurements for [G3]/[LiTf$_2$N] = 3/4 (at 70 °C) and [G4]/[LiTf$_2$N] = 3/5 (at 80 °C) were performed at 600 MHz using a JNM–ECA600 FT NMR spectrometer (JEOL Ltd.). The temperatures were selected so that the samples show similar viscosities of ~100 mPa s. By using double NMR tubes (Shigemi Corp., SC-002), samples were separated from the external standard. Dimethyl sulfoxide-d_6 (Cambridge Isotope Laboratories, Inc.) were placed in the outer tube (5.2 mmφ) and sample was added to the internal tube (5.0 mmφ). The self-diffusion coefficients of G5 (^{1}H), Li$^+$ (^{7}Li), and Tf$_2$N$^-$ (^{19}F) were measured using a simple Hahn spin echo sequence and analyzed using the Stejskal equation; $\ln(I/I_0) = -D(\gamma g \delta)^2(\Delta - \delta/3)$, where I is the echo signal intensity, I_0 is the initial echo signal intensity, D is the self-diffusion coefficient, γ is the gyromagnetic ratio (2.67515 × 10^8 rad s^{-1} T^{-1} for ^{1}H, 1.03966 × 10^8 rad s^{-1} T^{-1} for ^{7}Li, and 2.51716 × 10^8 rad s^{-1} T^{-1} for ^{19}F), g is the amplitude of the gradient pulses, δ is the duration of the gradient pulses, and Δ is the interval between the leading edges of the gradient pulses.[25] The g values used were in the range 10–850 mT m^{-1} for ^{1}H, ^{7}Li, and ^{19}F in the G3 and G4 samples. The value of δ was 4 ms and Δ was 100 ms.

The conductivity of [G3]/[LiTf$_2$N] = 3/4, [G4]/[LiTf$_2$N] = 3/5, and [G5]/[LiTf$_2$N] = 1/1 was determined by electrochemical impedance spectroscopy (Bio-Logic Science Instruments SAS, VSP-300) using a self-made teflon cell with stainless steel electrodes. The cell constant was calibrated with 0.1 and 1 mol dm^{-3} KCl aqueous solutions. The measurement was performed in a thermostatic chamber (Espec Co., SU-222) between 20 °C and 90 °C for [G3]/[LiTf$_2$N] = 3/4, between 35 °C and 90 °C for [G4]/[LiTf$_2$N] = 3/5. The conductivity was 7.75 mS cm^{-1} at 90 °C for [G5]/[LiTf$_2$N] = 1/1. Note that the G4 sample was not measured near room temperature (below 35 °C) as it may freeze during measurements. Viscosity measurements were performed between the same temperature ranges using a viscometer (Kyoto Electronics Manufacturing Co., Ltd., EMS-1000). Densities were calculated by using the measured values of weight and volume to be 1.55 g cm^{-3} at RT for [G3]/[LiTf$_2$N] = 3/4, 1.51 g cm^{-3} at RT for [G4]/[LiTf$_2$N] = 3/5, and 1.2 g cm^{-3} at 90 °C for [G5]/[LiTf$_2$N] = 1/1.

Transference number, denoted as $t_{Li+(EC)}$, was obtained by a chronoamperometry method using a Li metal|electrolyte|Li metal symmetric cell under Ar atmosphere. [G2]/[LiTf$_2$N] = 1/1 was measured at 30 °C, [G3]/[LiTf$_2$N] = 3/4 at 70 °C, [G4]/[LiTf$_2$N] = 3/5 at 80 °C, and [G5]/[LiTf$_2$N] = 1/1 at 90 °C. The temperatures were selected so that the samples show similar viscosities of ~100 mPa s, as was the case with the Raman and NMR measurements. Li metal foil was purchased from Honjo Metal and cut into a disk shape (16 mm in diameter and 0.5 mm thickness). A glass fiber filter (0.26 mm thickness) was inserted between the two Li metal electrodes as a separator. The Li metal electrodes and the electrolyte (ca. 0.5 ml) were encapsulated into a 2032-type coin cell, where the electrolyte was absorbed in the glass fiber filter. Electrochemical impedance spectra (EIS) were obtained in a frequency range of 1 MHz–100 mHz with a perturbation voltage amplitude of 10 mV, using a potentiostat (SP-200, BioLogic). To ensure the stabilization of Li electrode interface, EIS were preliminarily obtained before the potentiostatic polarization. Chronoamperometry was conducted with a potential step of 10 mV during the potentiostatic polarization. As prescribed in the literatures,[11,12,26] EIS were obtained again after the current reached the steady state i.e. under anion-blocking conditions.
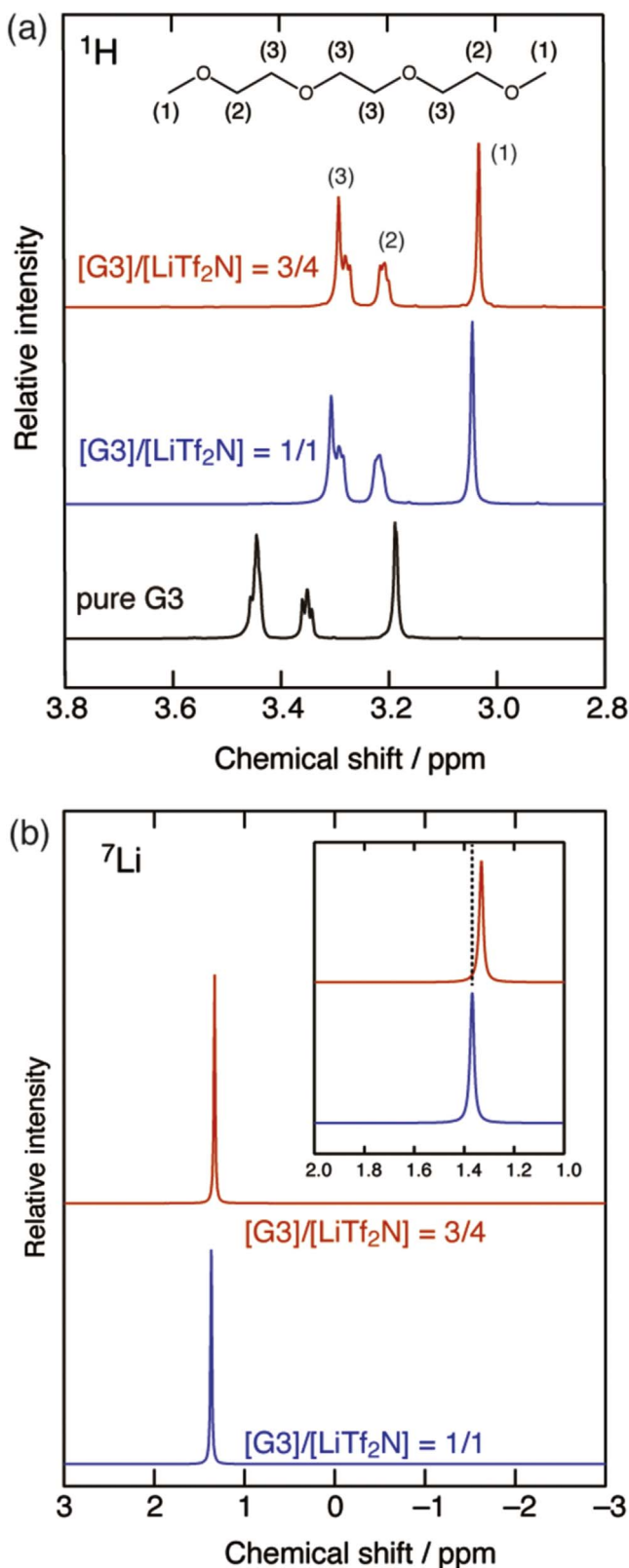
Figure 2. (a) ^{1}H NMR spectra for pure G3 and the molten states of [G3]/[LiTf$_2$N] = 3/4, 1/1, and (b) ^{7}Li NMR spectra for [G3]/[LiTf$_2$N] = 3/4, 1/1. Dashed lines are guide to the eye.

The cell exhibited a semicircle. The faradaic current is observed from the moment the voltage is applied, and the current decays and reached steady state.

Results and Discussion

Thermal properties.—The TG curves clearly show the better thermal stability when salts are added to the solvate ILs, i.e., [G3 or G4]/[LiTf$_2$N] = 1/1 (Figs. S1 and S2 available online at stacks.iop.org/JES/168/090521/mmedia; supplementary data). Compared with the solvate ILs, 5 wt% mass loss was observed at higher temperatures (208 °C for [G3]/[LiTf$_2$N] = 3/4 and 180 °C for [G3]/[LiTf$_2$N] = 1/1, and 248 °C for [G4]/[LiTf$_2$N] = 3/5 and 185 °C for [G4]/[LiTf$_2$N] = 1/1).

Among the glyme-LiTf$_2$N mixtures with [O]/[Li$^+$] = 3, the G3 mixture shows a property similar to the G5 mixture and contrast to the G2 mixture. The G2 mixture i.e., [G2]/[LiTf$_2$N] = 1/1 undergoes crystallization at T_m = 22 °C.[23,26] By contrast, [G3]/[LiTf$_2$N] = 3/4 only show glass transitions (T_g = –63 °C), similar to the case with [G5]/[LiTf$_2$N] = 1/2 (T_g = –54 °C).[12] The G4 sample freezes within several hours when kept near room temperature. Once the G4 sample was heated to melt, the sample showed a glass-forming liquid state at room temperature for a few hours. The DSC curves of the frozen G4 sample showed an endothermic peak at T_m = 55 °C for the 1st scan; however, the 2nd and 3rd scans show only a glass transition at T_g = –39 °C, when scanned between 90 °C and –90 °C at 5 °C min^{-1}.

Raman spectroscopy.—Figure 1 shows Raman spectra of [G3]/[LiTf$_2$N] = 3/4, 1/1, and pure G3. As shown in Fig. 1a, COC stretching and CH$_2$ rocking modes of oligoethers appear between 760 cm^{-1} and 900 cm^{-1}.[2,3,12,17,18,23] In the solvate IL, i.e., [G3]/[LiTf$_2$N] = 1/1, a peak appears at 872 cm^{-1}, proving a change from pure G3 as a result of G3-Li$^+$ complex formation similar to the literatures.[2,3,23] The Raman spectra of the super-concentrated electrolyte [G3]/[LiTf$_2$N] = 3/4 displayed a peak at 873 cm^{-1}, which also indicates complex formation. Similar features are observed for G4 (see Fig. S3; supplementary data). Moreover, the wavenumber of the peaks are 875 cm^{-1} for [G5]/[LiTf$_2$N] = 1/2, 873 cm^{-1} for [G3]/[LiTf$_2$N] = 3/4, and 869 cm^{-1} for [G4]/[LiTf$_2$N] = 3/5. Here, the optical resolution of the Raman system is 3 cm^{-1}. Consequently, the order of solvent-Li$^+$ interactions is G5 ≈ G3 > G4 (stronger to weaker), different from the order of the glyme chain length.

The CF$_3$ bending vibration and the S−N stretching vibration of Tf$_2$N$^-$ is a good indicator of the Li$^+$−Tf$_2$N$^-$ interactions. For LiTf$_2$N solvates, free or solvent separated ion pair (SSIP) type Tf$_2$N$^-$ anions show a band at 739−742 cm^{-1}, while contact ion pair (CIP) type and aggregate (AGG) type solvates show at higher frequencies (typically ⩾ 744 cm^{-1}).[2,12,23,27] In Fig. 1b, for [G3]/[LiTf$_2$N] = 3/4, the band appears at 748 cm^{-1}. In Fig. S4, for [G4]/[LiTf$_2$N] = 3/5, the band appears at 747 cm^{-1}. For [G3]/[LiTf$_2$N] = 1/1 and [G4]/[LiTf$_2$N] = 1/1, the peak appeared at lower wavenumbers (see Figs. 1b and S4). This strongly suggests that [G3]/[LiTf$_2$N] = 3/4 and [G4]/[LiTf$_2$N] = 3/5 form CIP or AGG type solvates, as well as the G5 system, due to their stronger cation–anion interactions than their equimolar counterparts.[12]

1D NMR spectroscopy.—Figures 2a and S5 show ^{1}H NMR spectra of the series of G3 and G4, respectively. The assignments of NMR signals are shown in the insets of Figs. 2a and S5. Compared to pure glymes, upfield shift is seen for the solvate ILs due to coordination to Li$^+$ ions. Also, upfield shift is observed for [O]/[Li$^+$] = 3 compared to the solvate ILs, indicating that each G3 or G4 solvent coordinates to more than one Li$^+$ ion for [O]/[Li$^+$] = 3, i.e., 4/3 li$^+$ ions for G3 and 5/3 li$^+$ ions for G4 in average.

Slight shift toward upfield compared with solvate ILs was also observed in the ^{7}Li NMR spectra. In Figs. 2b and S6, a singlet appears at 1.33 ppm for [G3]/[LiTf$_2$N] = 3/4 and 1.35 ppm for [G4]/[LiTf$_2$N] = 3/5, while it appears at 1.37 ppm and 1.46 ppm for the G3- and G4 solvate IL, respectively. In such G3- or G4-LiTf$_2$N mixture with excess LiTf$_2$N (ca. 5 mol% excess), formation of [Li(Tf$_2$N)$_2$]$^-$ was presumed.[28] However, no signal is seen below

0 ppm for [O]/[Li$^+$] = 3, even though the ^{7}Li NMR signal of [Li(Tf$_2$N)$_2$]$^-$ is reported to appear at –1.4 ppm.[29] Therefore, [Li(Tf$_2$N)$_2$]$^-$ anion is not dominant nor stable in [O]/[Li$^+$] = 3. Consequently, the slight upfield shift compared with solvate ILs is attributed to the stronger interactions between [Li$^+$·(glyme)] cation and Tf$_2$N$^-$ anion, rather than a coexistence of [Li(Tf$_2$N)$_2$]$^-$ and [Li$^+$·(glyme)].

For the G5 analogue, a singlet appears at 1.22 ppm for [G5]/[LiTf$_2$N] = 1/2 and 1.29 ppm for [G5]/[LiTf$_2$N] = 1/1.[12] The order of the ^{7}Li singlet is G5 > G3 > G4 (higher to lower field) for [O]/[Li$^+$] = 3. This is due to the stronger interactions of Li$^+$ with glymes and Tf$_2$N$^-$ anions, as demonstrated by the Raman results. Consequently, the super-concentrated G3, G4, and G5 solutions with [O]/[Li$^+$] = 3 consist of [Gn·(Li$^+$)$_m$] ($m > 1$) cations and Tf$_2$N$^-$ anions in CIP or AGG type. Notably, the densities of the longer glyme system are 1.51–1.56 g cm^{-3} at room temperature, 3%–6% larger than the G2 compound [G2]/[LiTf$_2$N] = 1/1 (1.468 g cm^{-3} as reported in Ref. 23). The larger density for the longer glyme system reflects the solvent-Li$^+$ and Li$^+$-Tf$_2$N$^-$ interactions. Since G2 cannot link two Li$^+$ at [O]/[Li$^+$] = 3, the interactions—the solvent-Li$^+$ interaction rather than the Li$^+$-Tf$_2$N$^-$ interaction— are smaller in the G2 system.

Observation of hopping conduction by self-diffusion coefficients.—Figure 3 shows PFSE-NMR results for Li$^+$, Tf$_2$N$^-$, and glyme of [G3]/[LiTf$_2$N] = 3/4 and [G4]/[LiTf$_2$N] = 3/5. The plots of echo signal attenuation on the basis of the Stejskal equation had linear relationships. According to the Stejskal equation, the gradients of the fitted lines are proportional to the self-diffusion coefficients. Table I lists the estimated values of self-diffusion coefficients of glyme (D_{glyme}), Li$^+$ (D_{Li+}), and Tf$_2$N$^-$ (D_{Tf2N-}). The ratio D_{Li+}/D_{glyme} is 1.8 for G3 and 1.5 for G4, evidencing hopping or ligand exchange conduction of Li$^+$ ions in the bulk electrolytes, as well as G5 (D_{Li+}/D_{glyme} = 2.0; Ref. 12). By contrast, ligand exchange conduction is absent (D_{Li+}/D_{glyme} = 1) for G2 with [O]/[Li$^+$] = 3 or [G2]/[LiTf$_2$N] = 1/1.[23,24] Since the coordination number of Li$^+$ is 4 or 5, one anion and at least 3 ether oxygens are necessary for the coordination. The schematic drawings of [Li$^+$·glyme] conduction for G2 and G3 are illustrated in Fig. 4. Here, G2, which has only 3 ether oxygens, cannot bridge two Li$^+$ ions to cause hopping conduction and only vehicular conduction

takes place (see Fig. 4, upper panel). By contrast, G3, which has more than three ether oxygens per molecule, can sometimes bridge two Li$^+$ ions to cause hopping conduction, otherwise form a chelate with one Li$^+$ ion to cause vehicular conduction (see Fig. 4, lower panel). The only one increase of ether oxygens per molecule, i.e. from G2 to G3, drastically changes the conduction behaviors.

It is noteworthy that the segmental motion of CH$_2$CH$_2$O moiety may be important for the hopping conduction observed in the super-concentrated G3 and G4 electrolytes. Actually, the segmental motion is active even for the short G3, as previously proved by spin-lattice relaxation time (T_1) measurements for lower concentrations ([O]/[Li$^+$] = 21 and 11, or [G3]/[LiTf$_2$N] = 21/4 and 11/4).[30] Interestingly, through the T_1 measurements at the low concentrations, Li$^+$ hopping conduction —activated by the segmental motion — was detected; however, the net Li$^+$ self-diffusion is *slower* than glymes and Tf$_2$N$^-$ anion ($D_{Li+} < D_{Tf2N-} < D_{glyme}$) due to the faster translational motion of free glymes.[30] When free glymes are absent, i.e., in solvate ILs of [Glyme]/[LiTf$_2$N] = 1/1, the values of D_{Li+} and D_{glyme} becomes identical; however, the hopping conduction by the segmental motion is still not apparent and the chelating effect of glymes is dominant to cause vehicular conduction. By contrast, the super-concentrated electrolyte solutions ([O]/[Li$^+$] = 3) show the apparent hopping conduction. This is because the chelating is partially replaced by bridging (see Fig. 4, lower panel).

Ligand exchange conduction is not so special in polyether systems such as polyethylene oxide (PEO; H(OCH$_2$CH$_2$)$_n$OH).[31,32] In those systems, Li$^+$ ions hop via the segmental motion of CH$_2$CH$_2$O moiety rather than Stokes-like vehicular conduction with PEO. Note, however, Li$^+$ generally diffuses slower than Tf$_2$N$^-$ anion in the polymer electrolytes,[30] while Li$^+$ diffuses faster in the glyme-based super-concentrated electrolyte.

Walden plots.—Figure 5 displays the Walden plots, plots of molar conductivity (Λ_{imp}/S cm^2 mol^{-1}) vs fluidity (η^{-1}/Poise^{-1}; 1 Poise = 100 mPa s) for the series of [O]/[Li$^+$] = 3. The raw data, i.e., conductivities and viscosities of the [G3]/[LiTf$_2$N] = 3/4 and [G4]/[LiTf$_2$N] = 3/5 are listed in Tables SI and SII. The molar conductivities Λ_{imp} are defined as $\Lambda_{imp} = M\sigma/d$, where σ is the conductivity measured by the electrochemical impedance method, d is density (1.55 g cm^{-3} for [G3]/[LiTf$_2$N] = 3/4 and 1.51 g cm^{-3} for [G4]/[LiTf$_2$N] = 3/5), and M is molecular weight (561.04 g mol^{-1}
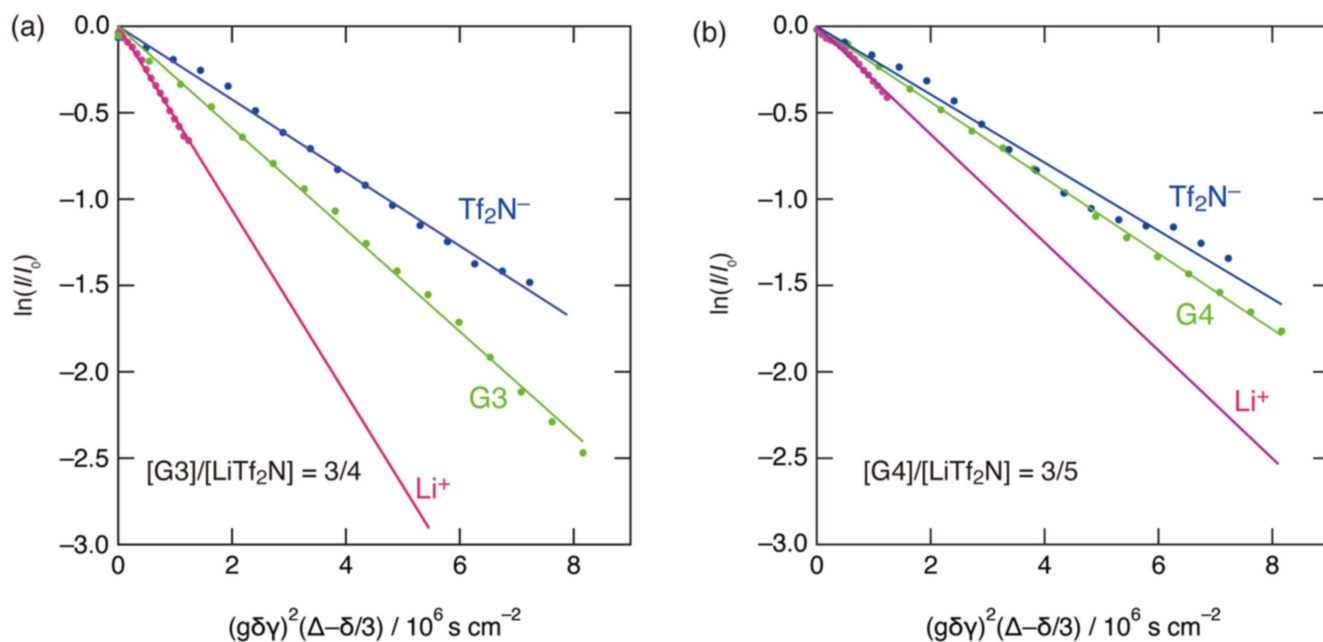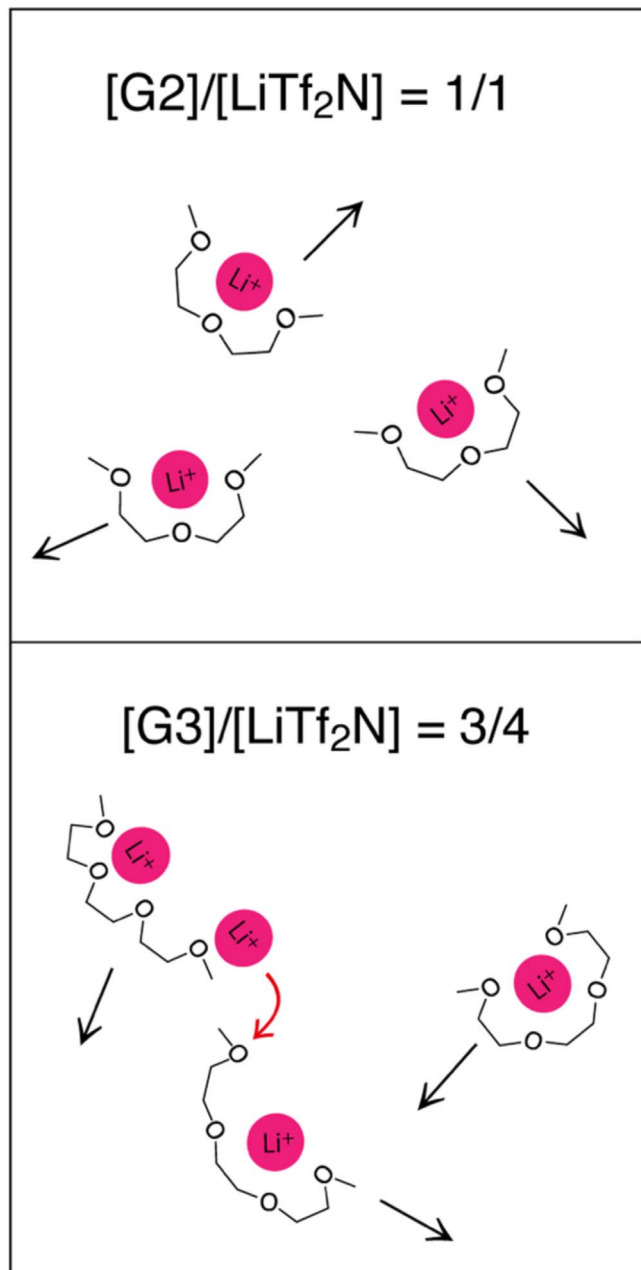
Figure 3. Plots of echo signal attenuation on the basis of the Stejskal equation for Li$^+$ (purple circles), Tf$_2$N$^-$ (blue circles), and G3 or G4 (green circles) of the molten glyme-Li$^+$ salt solvates, (a) [G3]/[LiTf$_2$N] = 3/4 and (b) [G4]/[LiTf$_2$N] = 3/5.
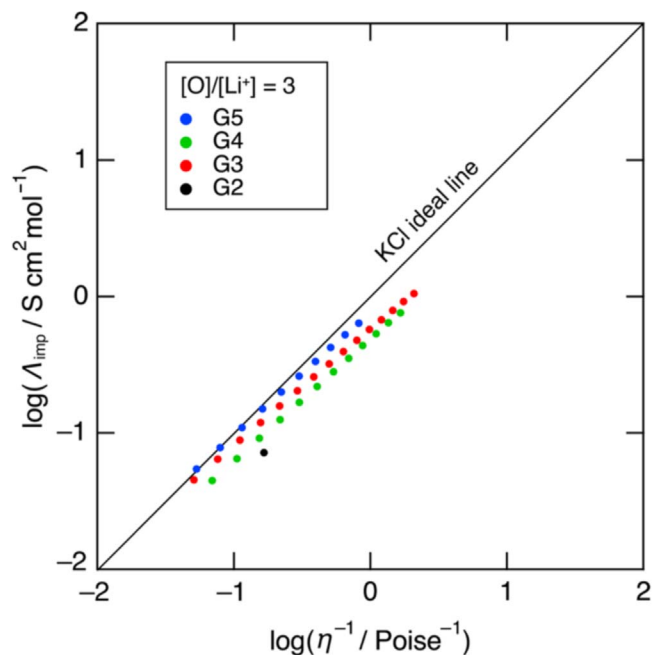
Table I. Self-diffusion coefficients for the glyme-LiTf$_2$N electrolytes with [O]/[Li$^+$] = 3.

composition	Self-diffusion coefficients (10^{-7} cm^2 s^{-1})		
	D_{glyme}	D_{Li+}	D_{Tf2N-}
[G5]/[LiTf$_2$N] = 1/2 (70 °C)[a]	0.56	1.1	0.67
[G4]/[LiTf$_2$N] = 3/5 (80 °C)	2.2	3.2	1.9
[G3]/[LiTf$_2$N] = 3/4 (70 °C)	2.9	5.3	2.1
[G2]/[LiTf$_2$N] = 1/1 (30 °C)[b]	0.22	0.21	0.16

a) Ref. 12. b) Ref. 23.

Figure 5. Walden plots of Glyme-LiTf$_2$N systems with [O]/[Li$^+$] = 3. [G5]/[LiTf$_2$N] = 1/2 (data from Ref. 12) and [G2]/[LiTf$_2$N] = 1/1 (data from Ref. 23) are also plotted.

Figure 4. Schematic drawings of G2-LiTf$_2$N mixture (upper panel) and G3-LiTf$_2$N mixture (lower panel) with the ratio [O]/[Li$^+$] = 3. Tf$_2$N$^-$ anions are omitted for clarity.

for [G3]/[LiTf$_2$N] = 3/4 and 700.79 g mol^{-1} for [G4]/[LiTf$_2$N] = 3/5). The ideal molar conductivity, Λ_{ideal}, is the value at a given fluidity of an ideal KCl aqueous solution, that is, the absolute values of Λ_{ideal} is equal to those of fluidity. Data for [G2]/[LiTf$_2$N] = 1/1 and [G5]/[LiTf$_2$N] = 1/2 are also plotted.[12,23] For G5, Λ_{imp} mostly overlap the ideal line, like in the other concentrated electrolytes where hopping conduction takes place.[10,11] By contrast, for [G2]/[LiTf$_2$N] = 1/1, where hopping conduction does not occur, Λ_{imp} are distancing from the ideal line ($\Delta W = -\log[\Lambda_{imp}/\Lambda_{ideal}] = 0.36$).[23] The Λ_{imp} values of [G3]/[LiTf$_2$N] = 3/4 and [G4]/[LiTf$_2$N] = 3/5 locate between the G5 and G2. For G3, Λ_{imp} approach the ideal line closely within the measured temperature range. In both cases, ΔW is smaller than the G2 system, likely due to the hopping conduction. The order of Λ_{imp} in the Walden plots is G5 > G3 > G4, in agreement with the other orders observed in Raman and NMR We also note that the order of the density at RT is also G5 (1.56 g cm^{-3}) > G3 (1.55 g cm^{-3}) > G4 (1.51 g cm^{-3}), although the molar volumes are in the order of G5 (840.55 g mol^{-1}/1.56 g cm^{-3}) > G4 (700.79 g mol^{-1}/1.51 g cm^{-3}) > G3 (561.04 g mol^{-1}/1.55 g cm^{-3}). The results strongly suggests a correlation between the coordination structure and the transport properties.

Classification by iconicity.—Ionicity is expressed as a molar conductivity ratio $\Lambda_{imp}/\Lambda_{NMR}$.[15–18,23,24,33,34] This is a useful metric for evaluating the extent to which the self-diffusion of ionic species (Λ_{NMR}) contributes to the actual ionic conduction (Λ_{imp}). The molar conductivity Λ_{NMR} is given by the Nernst-Einstein equation, $\Lambda_{NMR} = (F^2/RT)(D_{cation} + D_{anion})$, where F is Faraday constant, R is the gas constant, T is the absolute temperature. The ionicity

stands for the deviation of Λ_{imp} from the "ideal" molar conductivity Λ_{NMR}, because ion correlations are ignored in the Nernst-Einstein equation by assuming that each ion moves independently without any interionic interactions.[33–35] By mapping in transport properties (e.g., D_{Li+}/D_{glyme} and $t_{Li+(EC)}$) vs ionicity, a series of related electrolytes can be classified.[23,24,33]

Figure 6 shows the plots of D_{Li+}/D_{glyme} vs ionicity for Glyme-LiTf$_2$N systems, the values of which are listed in Table SIII (see supplementary data). In [Glyme]/[LiTf$_2$N] = 1/1 (including the G2 compound), where hopping conduction does not occur (D_{Li+}/D_{glyme} = 1), the ratio $\Lambda_{imp}/\Lambda_{NMR}$ is relatively high to exceed 0.4.[24] By contrast, the super-concentrated electrolyte solutions of [O]/[Li$^+$] = 3 (except the G2 compound), locate along ionicity $\sim$ 0.2 with D_{Li+}/D_{glyme} > 1. As shown, among [O]/[Li$^+$] = 3 a clear line can be drawn between G2 and glymes longer than G2. In addition, the magnitude of D_{Li+}/D_{glyme} is in the order G5 > G3 > G4, similar to the Raman and 1D NMR results.

The transference numbers $t_{Li+(EC)}$ are also plotted against ionicity (Fig. 7). The values of $t_{Li+(EC)}$ are listed in Table SIII (see supplementary data). The current-time plots and time-dependent EIS for the Li|electrolyte|Li cell are supplemented as Figs. S7–S10 (see supplementary data). Significantly low $t_{Li+(EC)}$ values have been reported for the solvate ILs, where the high stability of the Li$^+$-glyme solvate cations inhibits momentum exchange of Li$^+$ ions.[36] By contrast, the super-concentrated, LiTf$_2$N-rich electrolytes ([Glyme]/[Li$^+$] < 1 in Fig. 7) show three to six times higher $t_{Li+(EC)}$ values. The correlations between D_{Li+}/D_{glyme} and $t_{Li+(EC)}$ are apparent while correlations between D_{Li+}/D_{Tf2N-} and $t_{Li+(EC)}$ are not. Thus, the hopping conduction i.e., the more-pronounced decoupling of Li$^+$ ion diffusion from solvents, may result in higher transference number than those for the solvate ILs. Notably, $t_{Li+(EC)}$ is nearly temperature-independent. For the super-concentrated G3 electrolyte, the $t_{Li+(EC)}$ was also measured at 30 °C; the value was 0.08, very similar to that at 70 °C (0.10). For G5, the $t_{Li+(EC)}$ is identical both at 70 °C and 25 °C.[12] The G4 sample was not measured near room temperature because the sample may freeze during measurements.

The order of $t_{Li+(EC)}$ is G5 (0.26) > G4 (0.18) > G3 (0.10) for the LiTf$_2$N-rich electrolytes ([Glyme]/[Li$^+$] < 1), showing the trend *different* from those observed in Raman, NMR, and Walden plots. One might possibly speculate that the longer glymes would give the higher transference numbers due to the more active segmental motions of the CH$_2$CH$_2$O moiety. However, a specific value is obtained for G2 (0.12). This relatively high value may be because the residence time of the [Li$^+$·G2] complex is short for such small ligands: according to the Bedrov's strategy for high $t_{Li+(EC)}$, short glymes such as G1 (n = 1) and G2 are effective for decreasing the residence time, although they demonstrated at [O]/[Li$^+$] = 4 or 5.[36] In any case, $t_{Li+(EC)}$ is essentially a dynamic index and strongly relates to the residence time, which do not necessarily reflects the static structure. Therefore, the order of $t_{Li+(EC)}$ for [O]/[Li$^+$] = 3 (including G2) showed the different trend. Molecular dynamics (MD) simulations for these system would be of interest.

Even though the order is different, another trend can be extracted. Compared at the same glyme chain length, the value of $t_{Li+(EC)}$ increases with decreasing ionicity. This trend has been recognized in the *equimolar* glyme–lithium salt mixtures of different anions, of which Lewis basicity varies from weak (bis(perfluorosulfonyl) amides such as Tf$_2$N$^-$) to strong (nitrate (NO$_3^-$), trifluoromethane-sulfonate (TfO$^-$), and trifluoroacetate (TFA$^-$)).[33] The equimolar mixtures with weakly Lewis basic anions shows high ionicity (> 0.4), i.e., solvate ILs, whereas those with strongly Lewis basic (SLB) anions show low ionicity, far from ideal solvate ILs.[24] Although there are no reports for SLB anions showing ionicity $\sim$ 0.2 in the equimolar mixtures, the combinations of ionicity and $t_{Li+(EC)}$ are approximately (0.06, 0.9) for TFA$^-$, (0.1, 0.7–0.8) for NO$_3^-$, and (0.3, 0.4) for TfO$^-$.[33] For the SLB anions, the strong cation–anion interactions cause AGG-type ion clusters, which induce the collective motions of cations and anions to lower ionicity
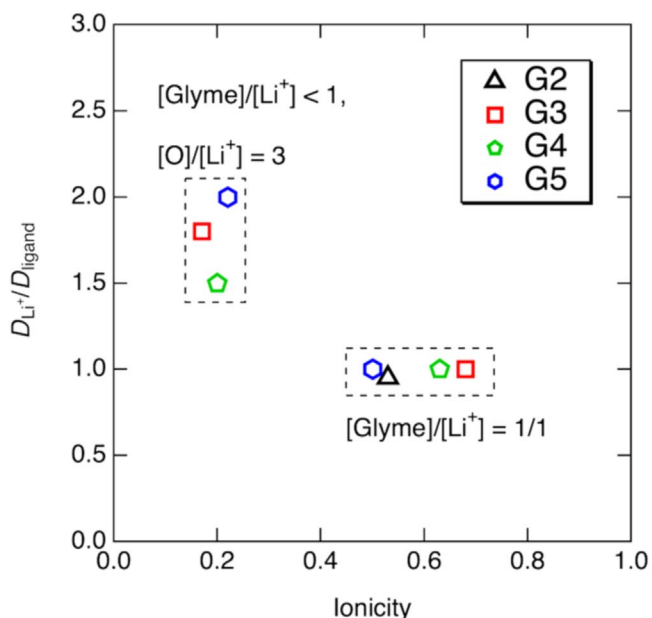

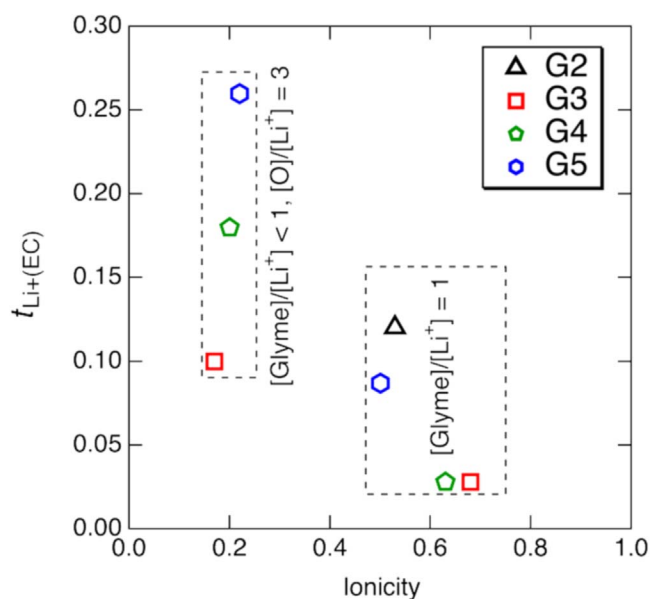**Figure 6.** Plots of D_{Li+}/D_{ligand} vs ionicity for the glyme-LiTf$_2$N systems.

Figure 7. Plots of $t_{Li+(EC)}$ vs ionicity for the glyme-LiTf$_2$N systems.

but to increase $t_{Li+(EC)}$ compared to the solvate ILs. The combination—strong cation–anion interactions, low ionicity, and relatively high $t_{Li+(EC)}$—are also the case with the LiTf$_2$N-rich system, as proved above. Therefore, we speculate that the AGG-anion cross-links Li$^+$ ions in the super-concentrated glyme-LiTf$_2$N system.

However, as represented by the contrast D_{Li+}/D_{glyme} ratio—between the equimolar glyme-SLB and the LiTf$_2$N-rich glyme system—their Li$^+$–glyme interactions are in stark contrast. In the SLB system, the glyme solvation is unstable and free (or highly exchangeable) glymes exist, giving D_{Li+}/D_{glyme} < 1.[24,33] For the LiTf$_2$N-rich system, by contrast, solvation is stable and free glymes are absent but D_{Li+}/D_{glyme} > 1, unlike the solvate ILs (D_{Li+}/D_{glyme} = 1). Although there are no free glymes, the salt addition to the solvate ILs "destabilize" [Li$^+$·glyme] complex, to give the bridging of two Li$^+$ instead of chelating of one Li$^+$ (see Fig. 4, lower panel). As a result, the residence time of Li$^+$ ions at solvents is reduced, giving the higher Li$^+$ transference numbers compared to

the solvate ILs. We also note that the super-concentrated glyme-LiTf$_2$N systems surpass solvate ILs in thermal stability (see Figs. S1 and S2), to say nothing of the equimolar glyme-lithium salt with the strongly basic anions which grant free glymes. Nonetheless, the transference numbers are still low ($t_{\mathrm{Li+(EC)}} = 0.08$ for G3, 0.18 for G4, and 0.26 for G5) in LiTf$_2$N-rich systems, possibly due to the presence of the strong Li$^+$–solvent interactions.

Consequently, even in glyme-LiTf$_2$N system $t_{\mathrm{Li+(EC)}}$ can be improved by salt addition to the solvate ILs, where the chelating is partially replaced by bridging. The super-concentrated glyme-LiTf$_2$N system and the equimolar SLB system is similar in that cation-anion interactions become stronger and the momentum exchange become easier than the equimolar glyme-LiTf$_2$N system or solvate ILs. However, the glyme-Li$^+$ interactions are in stark contrast and the absolute values of $t_{\mathrm{Li+(EC)}}$ is significantly different. Notably, high $t_{\mathrm{Li+(EC)}}$ (> 0.5) and $D_{\mathrm{Li+}}/D_{\mathrm{solvent}} > 1$ at high salt concentrations with AGG-type ion clusters has been realized in other solvents such as sulfolane,[26] which do not undergo chelate coordination because they have less than three coordination sites per molecule.

Conclusions

A series of super-concentrated electrolyte solutions of glyme-LiTf$_2$N with [O]/[Li$^+$] = 3 are investigated. A clear line can be drawn between G2 and the longer glymes. The clue for the hopping conduction is whether the number of coordination sites per ligand molecule is in excess or not. For example, sodium ions which have the coordination number of 5 would show contrast properties between G3 and the longer glymes. In terms of transport properties and ionicity, the super-concentrated electrolyte solutions of glyme-LiTf$_2$N ($D_{\mathrm{Li+}}/D_{\mathrm{glyme}} > 1$, high transference number, low ionicity) is distinguished not only from the solvate ILs ($D_{\mathrm{Li+}}/D_{\mathrm{glyme}} = 1$, low transference number, high ionicity) but also from equimolar glyme-lithium salt mixture with free glymes ($D_{\mathrm{Li+}}/D_{\mathrm{glyme}} < 1$, very high transference number, low ionicity). Even in the glyme-lithium salt system with weakly basic anions such as Tf$_2$N$^-$, transference number can definitely improve by the salt addition to the solvate ILs. These findings can be a guideline for designing glyme-based electrolytes.

Acknowledgments

ORCID

Atsushi Kitada https://orcid.org/0000-0002-4387-8687
Masahiro Shimizu https://orcid.org/0000-0003-1084-7486
Kazuhiro Fukami https://orcid.org/0000-0001-9120-5578
Kuniaki Murase https://orcid.org/0000-0002-7564-9416

References

1. Y. Yamada and A. Yamada, *J. Electrochem. Soc.*, **162**, A2406 (2015).
2. T. Mandai, K. Dokko, and M. Watanabe, *Chem. Rec.*, **18**, 1 (2018).
3. K. Yoshida, M. Nakamura, Y. Kazue, N. Tachikawa, S. Tsuzuki, S. Seki, K. Dokko, and M. Watanabe, *J. Am. Chem. Soc.*, **133**, 13121 (2011).
4. S. Terada, H. Susa, S. Tsuzuki, T. Mandai, K. Ueno, K. Dokko, and M. Watanabe, *J. Phys. Chem. C*, **122**, 16589 (2018).
5. S. Terada, K. Ikeda, K. Ueno, K. Dokko, and M. Watanabe, *Aust. J. Chem.*, **72**, 70 (2019).
6. J.-D. Xie, W. J. Liu, C. Li, J. Patra, Y. A. Gandomi, Q.-F. Dong, and J.-K. Chang, *Electrochim. Acta*, **319**, 625 (2019).
7. K. Dokko, D. Watanabe, Y. Ugata, M. L. Thomas, S. Tsuzuki, W. Shinoda, K. Hashimoto, K. Ueno, Y. Umebayashi, and M. Watanabe, *J. Phys. Chem. B*, **122**, 10736 (2018).
8. A. Nakanishi, K. Ueno, D. Watanabe, Y. Ugata, Y. Matsumae, J. Liu, M. L. Thomas, K. Dokko, and M. Watanabe, *J. Phys. Chem. C*, **123**, 14229 (2019).
9. S. Kondou, M. L. Thomas, T. Mandai, K. Ueno, K. Dokko, and M. Watanabe, *Phys. Chem. Chem. Phys.*, **21**, 5097 (2019).
10. Y. Ugata, M. L. Thomas, T. Mandai, K. Ueno, K. Dokko, and M. Watanabe, *Phys. Chem. Chem. Phys.*, **21**, 9759 (2019).
11. R. Tatara, S. Nishimura, Y. Okamoto, K. Ueno, M. Watanabe, and K. Dokko, *J. Phys. Chem. C*, **124**, 15800 (2020).
12. A. Kitada, K. Kawata, M. Shimizu, M. Saimura, T. Nagata, M. Katahira, K. Fukami, and K. Murase, *J. Electrochem. Soc.*, **168**, 016506 (2021).
13. A. Noda, M. A. B. H. Susan, K. Kudo, S. Mitsushima, K. Hayamizu, and M. Watanabe, *J. Phys. Chem. B*, **107**, 4024 (2003).
14. T. Yasuda and M. Watanabe, *MRS Bull.*, **38**, 560 (2013).
15. A. Kitada, K. Kintsu, S. Takeoka, K. Fukami, M. Saimura, T. Nagata, M. Katahira, and K. Murase, *J. Electrochem. Soc.*, **165**, H496 (2018).
16. K. Kawata, A. Kitada, N. Tsuchida, M. Saimura, T. Nagata, M. Katahira, K. Fukami, and K. Murase, *Phys. Chem. Chem. Phys.*, **23**, 449 (2021).
17. K. Kawata, A. Kitada, N. Tsuchida, M. Saimura, T. Nagata, M. Katahira, K. Fukami, and K. Murase, *J. Electrochem. Soc.*, **167**, 046508 (2020).
18. K. Kawata, A. Kitada, N. Tsuchida, M. Saimura, T. Nagata, M. Katahira, K. Fukami, and K. Murase, *J. Electrochem. Soc.*, **168**, 026515 (2021).
19. K. Adachi, A. Kitada, K. Fukami, and K. Murase, *J. Electrochem. Soc.*, **166**, D409 (2019).
20. K. Adachi, A. Kitada, K. Fukami, and K. Murase, *Electrochim. Acta*, **338**, 135873 (2020).
21. Z. Zhang, A. Kitada, S. Gao, K. Fukami, N. Tsuji, Z. Yao, and K. Murase, *ACS Appl. Mater. Interfaces*, **12**, 43289 (2020).
22. A. Kitada, M. Kurihara, R. Takai, K. Fukami, and K. Murase, *J. Surf. Finish. Soc. Jpn.*, **71**, 376 (2020).
23. C. Zhang, K. Ueno, A. Yamazaki, K. Yoshida, H. Moon, T. Mandai, Y. Umebayashi, K. Dokko, and M. Watanabe, *J. Phys. Chem. B*, **118**, 5144 (2014).
24. K. Ueno, K. Yoshida, M. Tsuchiya, N. Tachikawa, K. Dokko, and M. Watanabe, *J. Phys. Chem. B*, **116**, 11323 (2012).
25. Stejskal and J. E. Tanner, *J. Chem. Phys.*, **42**, 288 (1965).
26. K. Shigenobu, K. Dokko, M. Watanabe, and K. Ueno, *Phys. Chem. Chem. Phys.*, **22**, 15214 (2020).
27. Y. Umebayashi, T. Mitsugi, T. Fujimori, K. Fujii, R. Kanzaki, M. Takeuchi, and S. Ishiguro, *J. Phys. Chem. B*, **111**, 13028 (2007).
28. H. Hirayama, N. Tachikawa, K. Yoshii, M. Watanabe, and Y. Katayama, *Electrochemistry*, **83**, 824 (2015).
29. A. Shirai, K. Fujii, Y. Umebayashi, S. Ishiguro, and Y. Ikeda, *Anal. Sci.*, **24**, 1291 (2008).
30. K. Hayamizu, Y. Sugimoto, E. Akiba, Y. Aihara, T. Bando, and W. S. Price, *J. Phys. Chem. B*, **106**, 547 (2002).
31. K. M. Abraham and M. Alamgir, *J. Electrochem. Soc.*, **137**, 1657 (1990).
32. R. C. Agrawal and G. P. Pandey, *J. Phys. D: Appl. Phys.*, **41**, 223001 (2008).
33. K. Shigenobu, M. Shibata, K. Dokko, M. Watanabe, K. Fujii, and K. Ueno, *Phys. Chem. Chem. Phys.*, **23**, 2622 (2021).
34. S. Pfeifer, F. Ackermann, F. Sälzer, M. Schönhoff, and B. Roling, *Phys. Chem. Chem. Phys.*, **23**, 628 (2021).
35. A. France-Lanord and J. C. Grossman, *Phys. Rev. Lett.*, **122**, 136001 (2019).
36. D. Dong, F. Sälzer, B. Roling, and D. Bedrov, *Phys. Chem. Chem. Phys.*, **20**, 29174 (2018).